Article

Cell Reports

A Role for Timp3 in Microbiota-Driven Hepatic Steatosis and Metabolic Dysfunction

Graphical Abstract

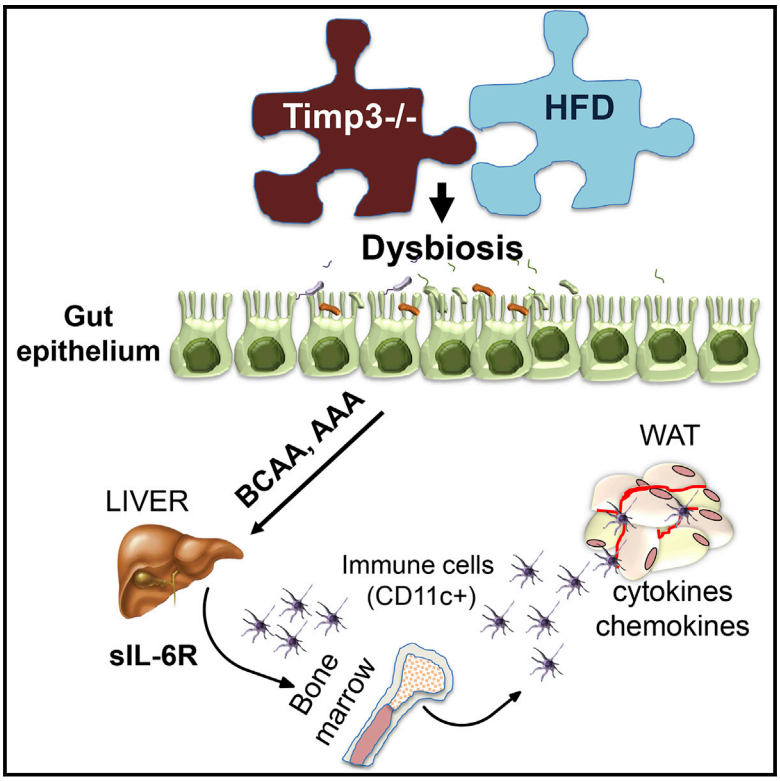

Authors

Maria Mavilio, Valentina Marchetti, Marta Fabrizi, ..., Remy Burcelin, Rossella Menghini, Massimo Federici

Correspondence

federicm@uniroma2.it

In Brief

Mavilio et al. show that Timp3 impacts gut-microbiome-related liver steatosis and glucose intolerance. Loss of Timp3 potentiates gut microbiota dysbiosis, leading to an increase in the development of inflammatory and metabolic abnormalities, which are mediated, in part, through IL-6 signaling. Antibiotic-mediated depletion of the microbiota improved these metabolic and inflammatory phenotypes.

Highlights

- Loss of Timp3 combined with an HFD affects glucose tolerance and innate immunity
- Timp3$^{-/-}$ mice exhibit gut dysbiosis, liver steatosis, and systemic inflammation
- Defective BCAA metabolism in Timp3$^{-/-}$ mice contributes to the metabolic phenotype
- Gut microbiome modulation by antibiotics rescues inflammatory and metabolic status

Mavilio et al., 2016, Cell Reports *16*, 731–743
July 19, 2016
http://dx.doi.org/10.1016/j.celrep.2016.06.027

Cell Reports
Article

A Role for Timp3 in Microbiota-Driven Hepatic Steatosis and Metabolic Dysfunction

Maria Mavilio,[1,7] Valentina Marchetti,[1,7] Marta Fabrizi,[1,2] Robert Stöhr,[1,3] Arianna Marino,[1] Viviana Casagrande,[1] Loredana Fiorentino,[1] Marina Cardellini,[1] Ben Kappel,[1,3] Ivan Monteleone,[4] Celine Garret,[5] Alessandro Mauriello,[4] Giovanni Monteleone,[1] Alessio Farcomeni,[6] Remy Burcelin,[6] Rossella Menghini,[1] and Massimo Federici[1,*]
[1]Department of Systems Medicine, University of Rome Tor Vergata, 00133 Rome, Italy
[2]Research Unit for Multi-Factorial Diseases, Obesity and Diabetes Scientific Directorate, Bambino Gesù Children Hospital, 00146 Rome, Italy
[3]Department of Internal Medicine I, University Hospital Aachen, 52074 Aachen, Germany
[4]Department of Biomedicine and Prevention, University of Rome Tor Vergata, 00173 Rome, Italy
[5]INSERM U1048, Université Paul Sabatier, IMC, 31432 Toulouse, France
[6]Department of Public Health and Infectious Diseases, Sapienza University of Rome, 00161 Rome, Italy
[7]Co-first author
*Correspondence: federicm@uniroma2.it
http://dx.doi.org/10.1016/j.celrep.2016.06.027

SUMMARY

The effect of gut microbiota on obesity and insulin resistance is now recognized, but the underlying host-dependent mechanisms remain poorly undefined. We find that tissue inhibitor of metalloproteinase 3 knockout (Timp3$^{-/-}$) mice fed a high-fat diet exhibit gut microbiota dysbiosis, an increase in branched chain and aromatic (BCAA) metabolites, liver steatosis, and an increase in circulating soluble IL-6 receptors (sIL6Rs). sIL6Rs can then activate inflammatory cells, such as CD11c^{+} cells, which drive metabolic inflammation. Depleting the microbiota through antibiotic treatment significantly improves glucose tolerance, hepatic steatosis, and systemic inflammation, and neutralizing sIL6R signaling reduces inflammation, but only mildly impacts glucose tolerance. Collectively, our results suggest that gut microbiota is the primary driver of the observed metabolic dysfunction, which is mediated, in part, through IL-6 signaling. Our findings also identify an important role for Timp3 in mediating the effect of the microbiota in metabolic diseases.

INTRODUCTION

The prevalence of obesity and its metabolic consequences, including type 2 Diabetes mellitus, non-alcoholic steatohepatitis, and cardiovascular diseases, is increasing worldwide (Anstee et al., 2013). Although genetics partially explain the new cases, there are environmental causes, including diet, physical activity, population density, and microbial exposure, that contribute to disrupting lipid and glucose metabolism (Tilg and Kaser, 2011). Several environmental inputs function through low-grade activation of chronic inflammatory pathways, provoking metabolic inflammation and related insulin resistance (Johnson and Olefsky, 2013; McNelis and Olefsky, 2014). However, both the source of the inflammatory burden and the extent to which inflammation primarily contributes to metabolic disorders are still unresolved (Ferrante, 2013). Recent studies have clearly identified the gut microbiota as an environmental factor that influences its host's metabolism to develop chronic metabolic disorders (Khan et al., 2014; Mehal, 2013; Moschen et al., 2013).

In previous studies from our laboratory we identified tissue inhibitor of metalloproteinase 3 (TIMP3), an extracellular matrix-bound metalloprotease with anti-inflammatory and anti-angiogenic properties, as an immunometabolic switch for inflammatory signals involved in metabolic phenotypes, such as glucose intolerance, reduced insulin action, and hepatic steatosis (Cardellini et al., 2009, 2011; Federici et al., 2005; Fiorentino et al., 2010; Menghini et al., 2009; Serino et al., 2007). The effect of Timp3 on metabolic homeostasis is thought to be a consequent of hyperactivation of inflammatory signals at the tissue level, particularly tumor necrosis factor alpha (TNF-α). In fact, TIMP3 modulates the activity of several matrix metalloproteinases (MMPs), including MMP9, MMP14, and the a disintegrin and metalloproteinase domain 17 (ADAM17), which, through the release of cytokine/chemokine factors, control immune cells trafficking in inflamed tissue to coordinate inflammation and tissue repair (Murphy et al., 2008).

Overexpression of Timp3 from monocyte CD68^{+} cells leads to the improvement of the metabolic syndrome phenotypes along with anti-inflammatory effects (Casagrande et al., 2012; Menghini et al., 2012).

Whether inflammation anticipates metabolic abnormalities in this model or vice versa is unresolved, and which factors anticipate the onset of the phenotype is still an unanswered question.

Coupling metabolome to metagenome profiling unveiled that the inflammatory glucose-intolerant status determined by the loss of Timp3 is related to dysbiosis at the gut level, and this is first reflected in liver steatosis and then systemically perpetrated via liver dependent release of sIL6R, which triggers metabolic inflammation through the mobilization of inflammatory cells, primarily CD11c^{+}, toward the adipose tissue.

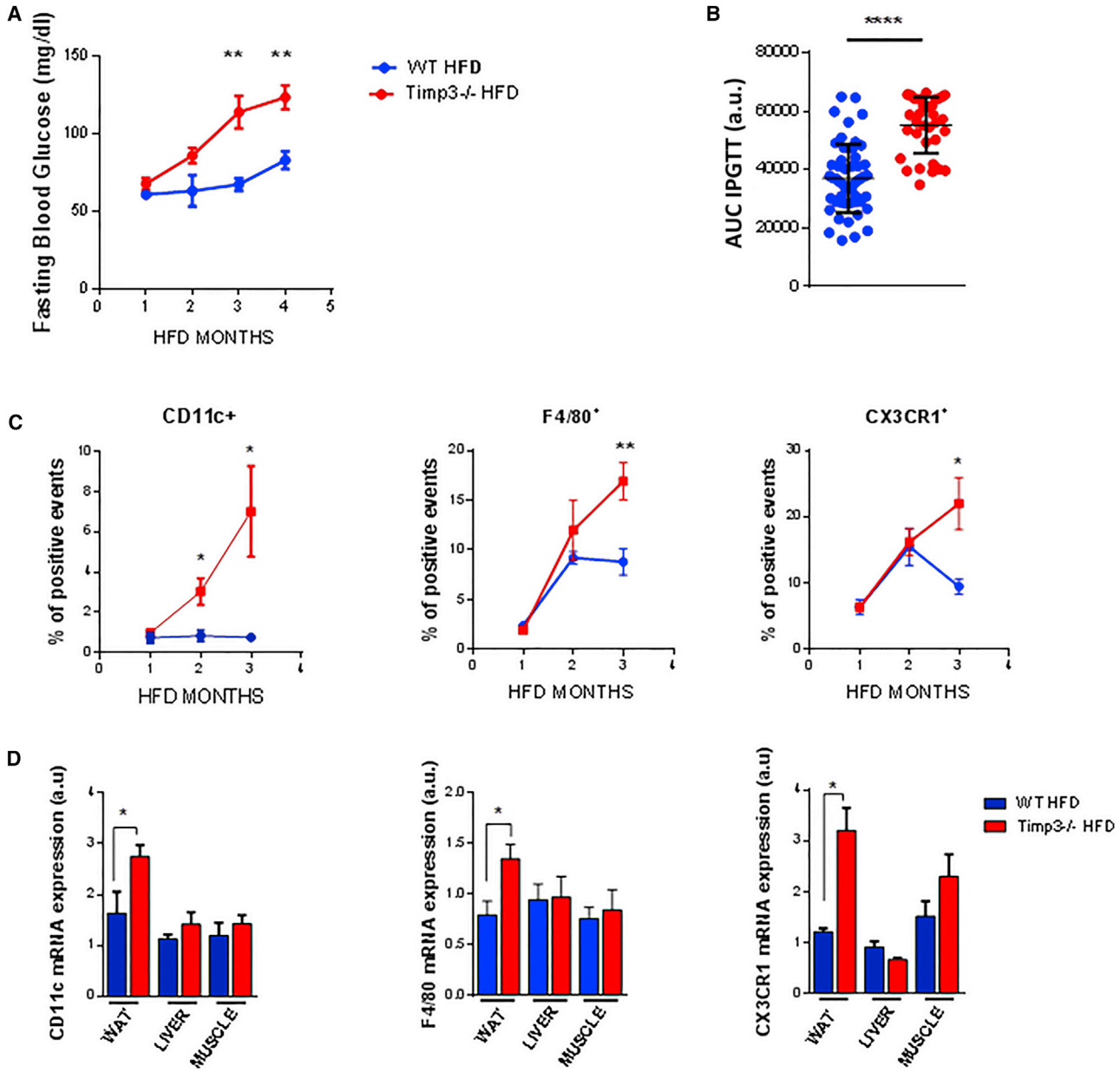

Figure 1. Metabolic Phenotyping of Timp3$^{-/-}$ Mice

(A) Fasting blood glucose levels were measured at different time points during an HFD (n = 5/each group; Student's t test with Welch's correction; **p < 0.01).

(B) Area under curve (AUC) during 120-min IPGTT of WT and Timp3$^{-/-}$ mice after 4 months on an HFD (n = 35/each group; data are mean ± SD, Student's t test with Welch's correction ****p < 0.0001).

(C) Flow cytometry analysis of blood leukocytes was performed using monoclonal antibodies directed against monocyte markers CD11c, F4/80, and CX3CR1 (n = 5 in each group; data are mean ± SEM; Student's t test with Welch's correction; *p < 0.05, **p < 0.01).

(D) mRNA expression of CD11c, F4/80, and CX3CR1 in white adipose tissue (WAT), liver, and muscle in WT and Timp3$^{-/-}$ animals at 4 months on an HFD. (n = 4 in each group; data are mean ± SEM; Student's t test with Welch's correction; *p < 0.05).

See also Figure S1.

RESULTS

Metabolic and Inflammatory Phenotype of Timp3$^{-/-}$ Mice

Our initial screening showed that combining the loss of Timp3 with a high-fat diet (HFD) resulted in a progressive rise in fasting blood glucose at 3 and 4 months (Figure 1A). After 4 months on an HFD, Timp3$^{-/-}$ mice had significantly higher glucose intolerance compared with wild-type (WT) mice as shown from an area under curve (AUC) calculation during an intraperitoneal glucose tolerance test (IPGTT) (Figure 1B). Timp3$^{-/-}$ mice fed an HFD showed a decrease in body weight, an increase in total

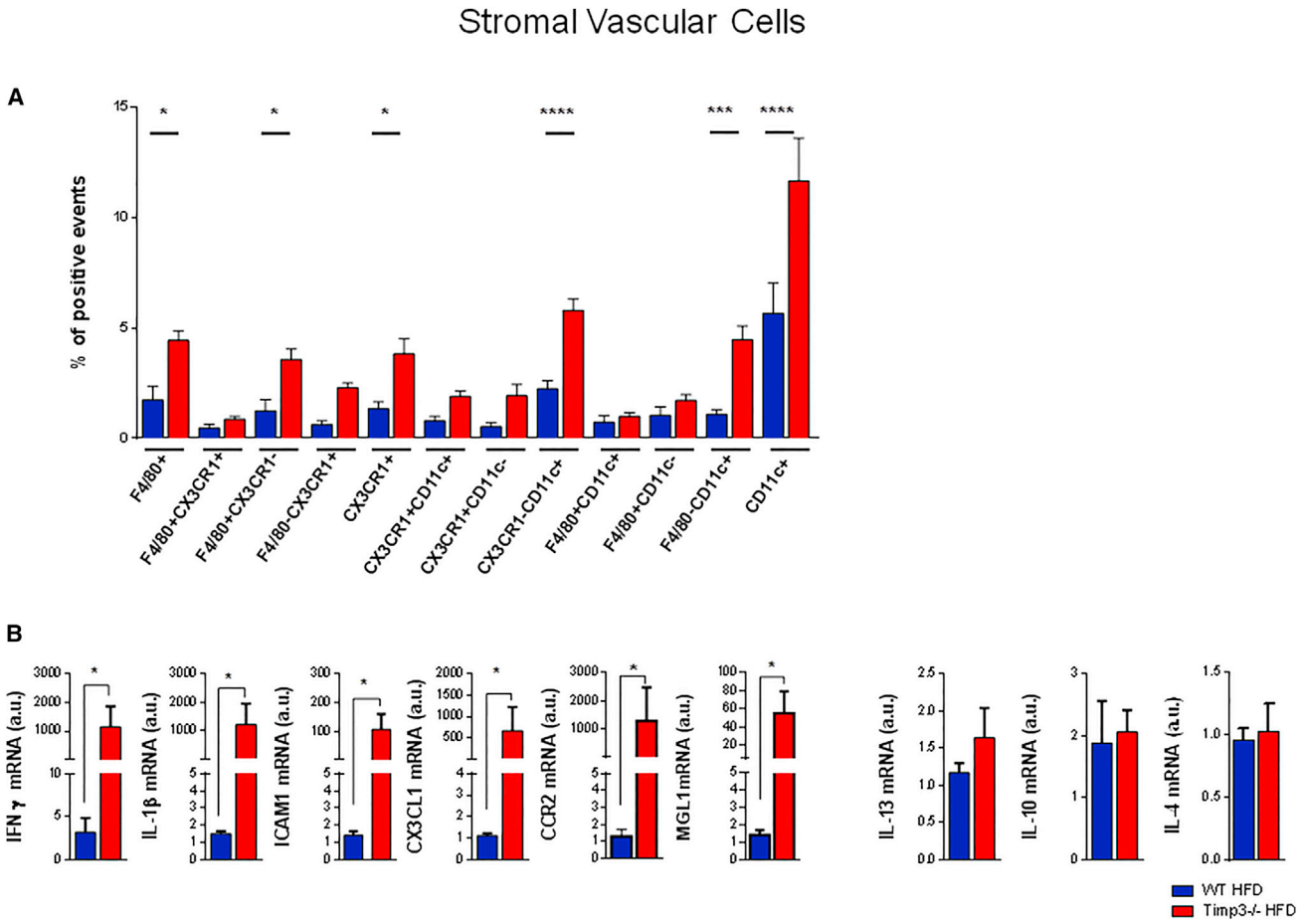

Figure 2. Inflammatory Phenotyping of Timp3$^{-/-}$ Mice

(A) Analysis of inflammatory infiltrate in the stromal vascular fraction (SVF) of WT and Timp3$^{-/-}$ animals after 4 months on an HFD (n = 5 in each group; data are mean ± SEM; *p < 0.05, ***p < 0.001, ****p < 0.0001 with one-way ANOVA with Sidak's multiple comparison test).

(B) Expression of pro- and anti-inflammatory genes in SVF from Timp3$^{-/-}$ mice and WT mice (n = 5 in each group; data are mean ± SEM; *p < 0.05 with Mann-Whitney t test).

See also Figure S2.

cholesterol, triglycerides, GOT-AST, and GPT-ALT, and an increase in ALT/AST ratio, all mildly significant compared with WT mice fed an HFD (Figures S1A and S1B). No difference was observed in energy expenditure parameters (Figure S1C).

Circulating proinflammatory cells positive to CD11c already increased at 2 months in Timp3$^{-/-}$ mice fed an HFD; this was followed by an increase in F4/80^{+} and CX3CR1^{+} cells (Figure 1C) at 3 months. Moreover, even several subpopulations of macrophage (F4/80^{+}CX3CR1^{-}; F4/80^{+}CX3CR1^{+}) and dendritic cells (CX3CR1^{+}CD11c^{+} and CX3CR1^{-} CD11c^{+}) were significantly increased (Figure S2A). Interestingly, analysis of the same markers in peripheral tissue revealed increased mRNA expression of CD11c, F4/80, and CX3CR1 in white adipose tissue (WAT), but not in liver and muscle from Timp3$^{-/-}$ mice compared with WT mice after 4 months on an HFD (Figure 1D). At the same time point, we analyzed the presence of proinflammatory leukocytes in the stromal vascular cells (SVCs) of WAT in WT and Timp3$^{-/-}$ animals. Cells expressing CD11c^{+}, F4/80^{+}, and CX3CR1^{+} were significantly increased (Figure 2A). mRNA expression of interferon gamma (IFNγ), the ligand for CX3CR1 (CX3CL1), interleukin 1 beta (IL1-β), the intercellular adhesion molecule 1 (ICAM1), macrophage galoctose-type C-type lectin 1(MGL1), and C-C chemokine Receptor type 2 (CCR2) were significantly overexpressed in Timp3$^{-/-}$ mice fed an HFD compared with the WT littermates fed an HFD without differences in anti-inflammatory cytokines, such as interleukin 10 (IL-10), interleukin 4 (IL-4), and interleukin 13 (IL-13) (Figure 2B). The adipose fraction in Timp3$^{-/-}$ mice fed an HFD showed no reduction in most of the analyzed metabolic genes, such as CCAAT/enhancer-binding protein beta (CEBP/β), CCAAT/enhancer-binding protein alpha (CEBP/α), glucose transporter type 4 (GLUT4), peroxisome proliferator-activated receptor gamma (PPARγ), hormone sensitive lipase (LIPE), adipose triglyceride lipase or patatin-like phospholipase domain-containing 2 (PNPLA2), insulin receptor (INSR), fatty acid binding protein 4 (FABP4), and diacylglycerol o-acyltransferase 1 (DGAT1)

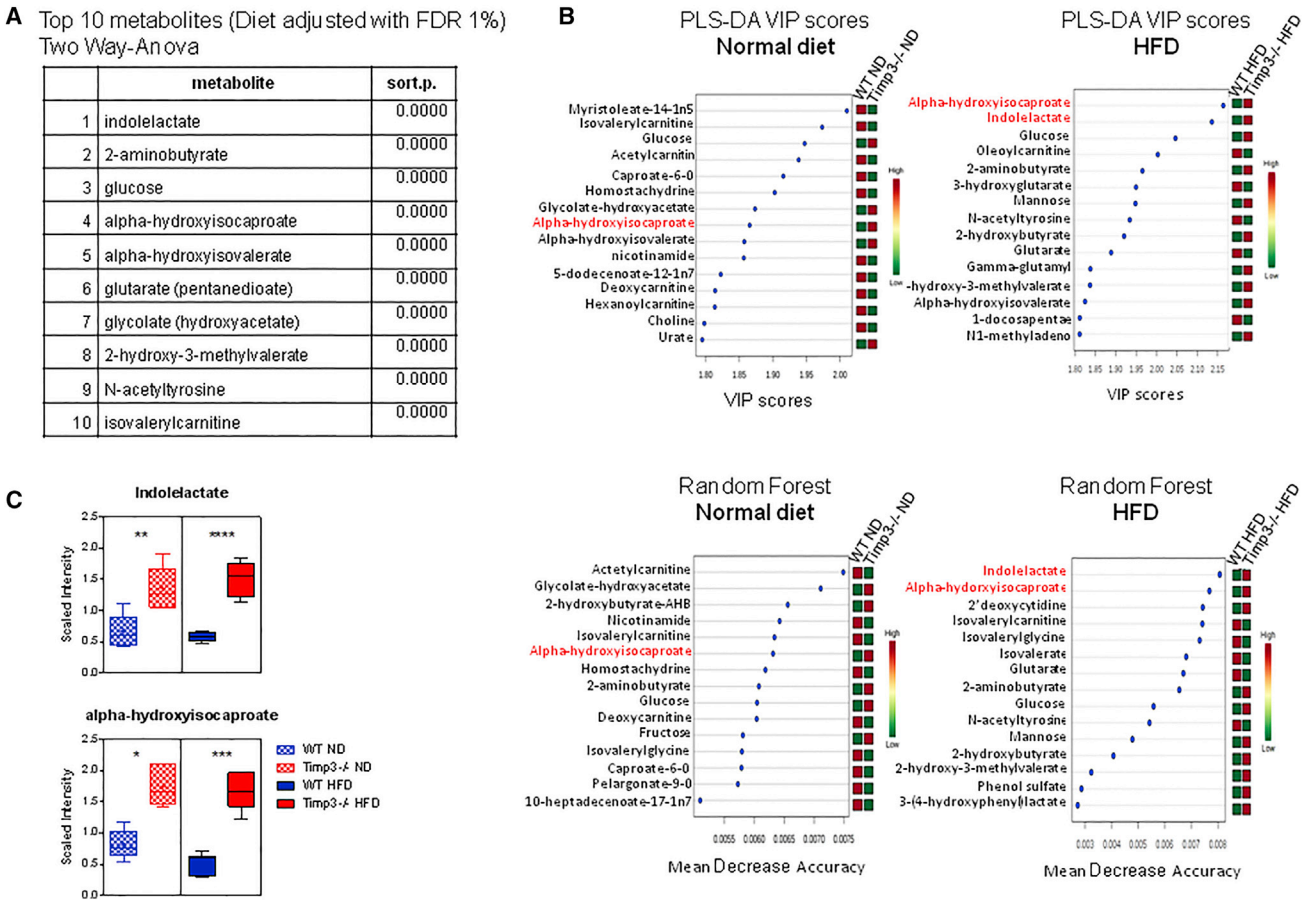

	metabolite	sort.p.
1	indolelactate	0.0000
2	2-aminobutyrate	0.0000
3	glucose	0.0000
4	alpha-hydroxyisocaproate	0.0000
5	alpha-hydroxyisovalerate	0.0000
6	glutarate (pentanedioate)	0.0000
7	glycolate (hydroxyacetate)	0.0000
8	2-hydroxy-3-methylvalerate	0.0000
9	N-acetyltyrosine	0.0000
10	isovalerylcarnitine	0.0000

Figure 3. Timp3$^{-/-}$ Mice Fed an HFD Have Altered BCAA and AAA Pathways

(A) Top-ten metabolites significantly different in Timp3$^{-/-}$ mice compared with WT mice in fasting state. Two-way ANOVA analysis adjusted for diet, with an FDR of 1%.

(B) PLS-DA (up) and random forest (down) approaches allowed to identify metabolites significantly different in Timp3$^{-/-}$ mice compared with WT mice on an ND or on an HFD in the fasting state.

(C) Two principal metabolites belonging to the BCAA and AAA pathways: alpha-hydroxyisocaproate and indolelactate are shown as box plots, with median, upper, and lower quartiles and maximum and mininum values in WT and Timp3$^{-/-}$ mice fed both an ND and an HFD in fasting state (n = 6 per group; one-way ANOVA with Sidak's multiple comparison test; *p < 0.05, **p < 0.01, ***p < 0.001****p < 0.0001).

See also Figures S3 and S5 and Tables S1, S2, and S3.

(Figure S2B). To understand which chemokine/cytokine may sustain increased inflammatory burden in Timp3$^{-/-}$ mice fed an HFD, we performed a large-scale cytokine profile. Serum cytokine array provided evidence for increased activity of the innate immune system, as evidenced by increased granulocyte-macrophage colony-stimulating factor (GM-CSF), monokine induced by gamma interferon (MIG), interleukin 6 (IL-6), and tumor necrosis factor alpha (TNF-α) in Timp3$^{-/-}$ mice fed an HFD compared with WT mice fed an HFD (Figure S2C).

These data show that the onset of inflammatory defects starts with or shortly anticipates overt glucose intolerance in this model and that this scenario is independent of obesity.

Metabolite Analysis Reveals Specific Defects in Timp3$^{-/-}$ Mice

To identify pathways linking inflammatory signals to metabolic derangements, we performed a global metabolome screening in serum from the fasting (ND and HFD) and fed state (HFD) mice using targeted liquid chromatography-tandem mass spectrometry (LC/MS-MS) and gas chromatography-mass spectrometry (GC-MS) analysis.

Metabolomics analysis in the fasting state comprises a total of 316 biochemicals (Table S1) with evidence of 100% predictive accuracy at the random forest (RF) confusion matrix in classifying groups into WT and Timp3$^{-/-}$ in both ND and HFD (Figure S3A). Two-way ANOVA analysis adjusted for diet and with a false discovery rate (FDR) of 1% revealed several metabolites that discriminate between WT and Timp3$^{-/-}$, including a few belonging to branched chain and aromatic amino acids (BCAA and AAA) metabolic pathways (Figures 3A, S3B, and S3C; Table S2).

Univariate analysis with PLS-DA and random forest approaches led to the identification of similar metabolites able to discriminate between WT and Timp3$^{-/-}$ mice fed an HFD

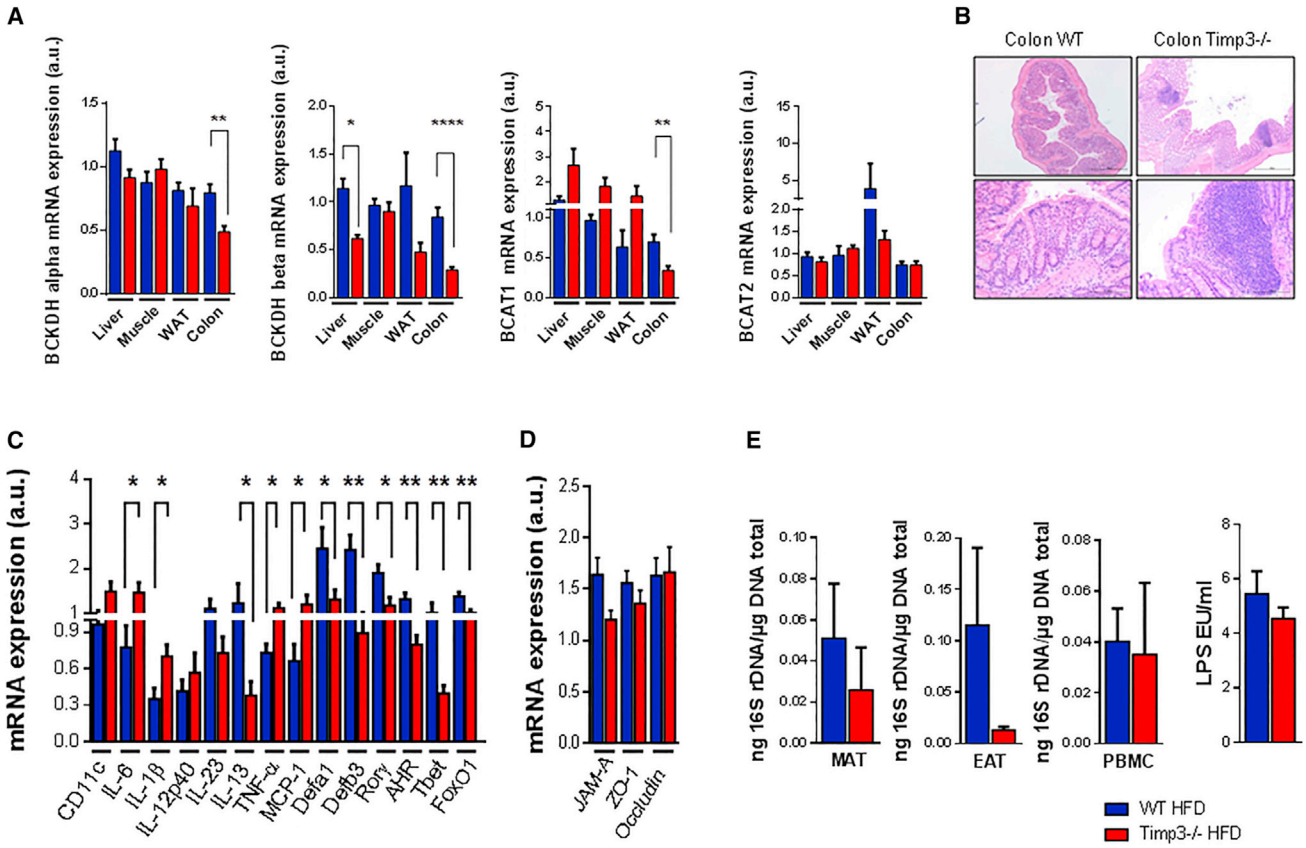

Figure 4. Timp3$^{-/-}$ Mice Fed an HFD Show Altered Expression for Metabolic and Inflammatory Signals in the Colon without Endotoxemia

(A) Real-time PCR analysis of RNA extracted from liver, muscle, white adipose tissue (WAT), and colon tissues of the Timp3$^{-/-}$ mice compared with the WT littermates fed an HFD. (n = 5 in liver, muscle, and WAT; n = 9 in colon; data are mean ± SEM; **p < 0.01, ****p < 0.0001 by Mann-Whitney t test; a.u.)

(B) H&E-stained colonic sections of WT and Timp3$^{-/-}$ mice at 4 months on an HFD. Upper, 4×; lower, 20×.

(C and D) Real-time PCR analysis on RNA extracted from colon tissue of the Timp3$^{-/-}$ mice compared with the WT littermates fed an HFD. (C) Inflammatory genes, (D) wall permeability genes. (n = 9 data are mean ± SEM; *p < 0.05, **p < 0.01 by Mann-Whitney t test).

(E) Quantification of 16S DNA concentrations in MAT (mesenteric adipose tissue), EAT (epididimal adipose tissue), and peripheral blood mononuclear cells (PBMCs) of Timp3$^{-/-}$ mice compared with WT animals. (n = 5 per group; data are mean ± SEM.) Serum levels of lipopolysaccharide (LPS) in WT and Timp3$^{-/-}$ mice fed an HFD (n = 10 per group).

See also Figure S4.

(fasted), with alpha-hydroxyisocaproate and indolelactate always as top predictors. The same analysis in WT and Timp3$^{-/-}$ mice under a ND showed that BCAA and AAA metabolic pathways slightly differed in the two strains, but only alpha-hydroxyisocaproate was among the top predictors in PLS-DA and random forest analysis (Figures 3B, 3C, and S3D).

This finding, again, suggests that a genotype/HFD interaction impinges on BCAA and AAA metabolic pathways.

To understand if the defective metabolism of BCAA could be explained by defects in the enzymes controlling the rate-limiting steps, we analyzed mRNA expression of the branched chain alpha-ketoacid dehydrogenase (BCKDH) complex and branched-chain-amino-acid transaminase (BCATm, encoded by BCAT2 gene) in the most metabolically active tissue, such as liver, muscle, WAT, and colon.

The colon is a highly metabolically active organ with functions not only for the remainder of the digestive tract, but also for the peripheral organs above mentioned.

In Timp3$^{-/-}$ mice fed an ND compared to WT mice fed an ND, we observed a significant decrease of BCKDH beta subunit in WAT and a modest decrease in muscle BCAT1 (Figure S4).

mRNA expression analysis of BCKDH isoforms in the metabolically active tissues revealed, on HFD challenge, a significant decrease, especially in the colon of Timp3$^{-/-}$ mice fed an HFD compared with WT mice fed an HFD, whereas no differences were found in BCAT1/2 mRNA expression (Figure 4A).

Given the fact that several metabolites varying between WT and Timp3$^{-/-}$ mice are derived from the gut microbiome, such as indole derivatives, we investigated whether loss of Timp3 has an impact on gut inflammation, permeability, and gut microbiota composition.

At the colon level, Timp3$^{-/-}$ mice fed an HFD revealed increased evidence for inflammatory activation, including massive lymphoid infiltrate, as evidenced by H&E staining (Figure 4B). At the molecular level, we observed altered innate immune genes. In particular, we detected an increased expression

of interleukin 1 beta (IL-1β), interleukin 6 (IL-6), TNF-α, and monocyte chemotactic protein 1 (MCP-1), whereas we found a significantly decreased expression of interleukin 13 (IL-13) and defensins, such as as Defa-1, Defb-3, as well as altered acquired immunity genes, such as decreased expression of the aryl hydrocarbon receptor (AHR), RAR-related orphan receptor gamma (Rorγ), and Forkhead box protein O1 (FoxO1) in Timp3$^{-/-}$ mice fed an HFD compared with WT mice fed an HFD (Figure 4C). No changes were observed in genes related to gut permeability, such as JAM-A, ZO-1, and Occludin (Figure 4D). Further, we did not observe differences in the analysis of bacterial translocation in mesenteric adipose tissue (MAT), epididimal adipose tissue (EAT), and peripheral blood mononuclear cells (PBMCs) or in the serum levels of lipopolysaccharide (LPS) (Figure 4E).

Overall, these data suggest the Timp3/HFD interaction induces gut microbiome dysbiosis, resulting in the generation of signals at the gut level that could influence systemic metabolic functions, including glucose tolerance. To corroborate this hypothesis, we performed a second experiment with Timp3$^{-/-}$ and WT mice fed a ND or an HFD. However, to have sufficient material for 16S metagenomics, mice were sacrificed in the fed state. Since we previously found the main differences in HFD, we also performed another metabolomics screening to be able to compare metabolites and 16S metagenomics in the same mice at the same time point (Table S3). PLS-DA, random forest, and functional class scoring analysis again revealed metabolites and metabolic pathways linked to BCAA (isoleucine, leucine, and valine metabolic pathways), as well as AAA (tryptophan pathway) (Figures S5A–S5C).

Because of our findings that several metabolites, particularly AAA derivatives, are gut microbiome dependent, we performed analysis comparing 16S bacterial DNA at the caecal level in Timp3$^{-/-}$ and WT mice, in both ND and HFD conditions (Tables S4, S5, S6, S7, and S8). At the phylum level we observed differences, particularly in the ND state (Figure S6). Because the metabolic phenotypes were evident on interaction of the loss of Timp3 and HFD, we focused particularly on this context. Analysis of families and genera revealed several differences with consistent modulation in *Mycoplasmataceae/Mycoplasma*, *Prevotellaceae/Prevotella*, *Sphingomonadaceae/Sphingomonas*, *Pasteurellaceae/Pasteurella, Helicobacteraceae/Helicobacter*, *Oxalobacteraceae/Massilia*, and *Lactobacillaceae/Lactobacillus* (Tables S4, S5, and S6). The first two were also evident when comparing WT and Timp3$^{-/-}$ mice fed an ND (Tables S7 and S8).

To investigate whether gut microbiota contributes to the inflammatory and diabetic phenotype observed in Timp3$^{-/-}$ mice and to test the relevance of our findings in a clinical perspective, we performed two different treatments in both WT mice fed an HFD and Timp3$^{-/-}$ mice fed an HFD.

In the first approach, we modulated the microbiota in WT mice fed an HFD and Timp3$^{-/-}$ littermates fed an HFD using a combination of broad-range antibiotics for 4 weeks (Abx) (ampicillin/metronidazole/norfloxacin 1g/l in drinking water). Results showed improved fasting and fed blood glucose levels and glucose tolerance in antibiotic-treated Timp3$^{-/-}$ mice fed an HFD, compared with untreated Timp3$^{-/-}$ mice fed an HFD (Figures 5A and 5B). Since Timp3$^{-/-}$ mice fed an HFD show liver steatosis (Fiorentino et al., 2010) and signs of non-viral hepatitis, we analyzed liver histology. Surprisingly, we observed that Abx treatment improved microvescicular, macrovescicular, and lobular inflammation, as well as improved ADAM17 convertase and MMPs activities (Figures 5E and S7A), in Timp3$^{-/-}$ mice fed an HFD compared with WT mice fed an HFD (Figures 5C and 5D). Remarkably, the BCKDH subunits of mRNA expression in liver and colon after Abx treatment were significantly improved in Timp3$^{-/-}$ mice fed an HFD (Figures 5F and 5G).

Next, we looked for agents that could translate the effect of dysbiosis at the systemic level. IL-6 was the most significantly increased cytokine in Timp3$^{-/-}$ mice fed an HFD (Figure S2C), and loss of Timp3 may potentially increase, via ADAM17, the soluble form of the IL-6 receptor (sIL6R) from liver and other tissues (Scheller et al., 2014; Schumacher et al., 2015; Yan et al., 2016). Our results confirmed that Timp3$^{-/-}$ mice fed an HFD showed significantly increased levels of IL-6, sIL6R, and IL-6/sIL6R interaction in serum (Figure 6A), as well as significantly increased levels of IL-6 in liver and WAT (Figure 6B).

Therefore, in the second approach we tested the hypothesis that dysbiosis in Timp3$^{-/-}$ mice was responsible for the increase of the IL-6/sIL6R complex and, in turn, for myeloid cells trafficking. When IL-6 binds to its soluble receptor, a trans-signaling alternative pathway is engaged, recruiting proinflammatory cells and amplifying the inflammatory cascade in several diseases (Scheller et al., 2014).

First, we investigated the levels of both IL-6 and soluble IL6-Ralpha in a serum sample of Timp3$^{-/-}$ and WT mice fed an HFD and subjected to antibiotic treatment compared with untreated samples.

We found decreased expression of both the soluble IL6R and IL-6 in treated compared with untreated samples serum from Timp3$^{-/-}$ mice fed an HFD, while no change was observed in the WT serum samples (untreated versus treated) (Figures 6C and 6D). Similar results were observed in analysis of CD11c^{+} circulating cells in blood and SVC derived from WAT (Figure 6E), in Timp3$^{-/-}$ mice fed an HFD and treated with Abx compared to untreated Timp3$^{-/-}$ mice fed an HFD and no differences between the two WT groups.

These data suggest that the gut microbiome possibly influences the sIL6R-CD11c^{+} axis via hepatic steatosis. However, whether these effects entirely depend on the gut microbiome and the associated dysbiosis or low-grade inflammation of the liver could not be revealed by this experiment. To elucidate this issue, we performed an intervention experiment to block the gut microbiome/liver-sIL6R-CD11c^{+} axis specifically in the second part (from liver to periphery) using soluble gp130Fc, a decoy protein that blocks IL-6/sIL6R trans-signaling. Treatment with soluble gp130Fc (sgp130Fc) improved fasting glycaemia after 1 month, glucose tolerance, and fasting insulin at 2 months after injection in Timp3$^{-/-}$ mice compared to untreated Timp3$^{-/-}$ mice (Figures 7A and 7B, respectively).

In Timp3$^{-/-}$ mice treated with sgp130Fc we found a decreased number of circulating CD11c^{+} cells and several proinflammatory subpopulations in the blood at 1 month and in SVC at 2 months from injection, while no differences were observed in the blood at 2 months from injection in either Timp3$^{-/-}$ or WT mice (Figures 7C–7F). Consistent with our hypothesis, treatment with sgp130Fc did not improve features of liver

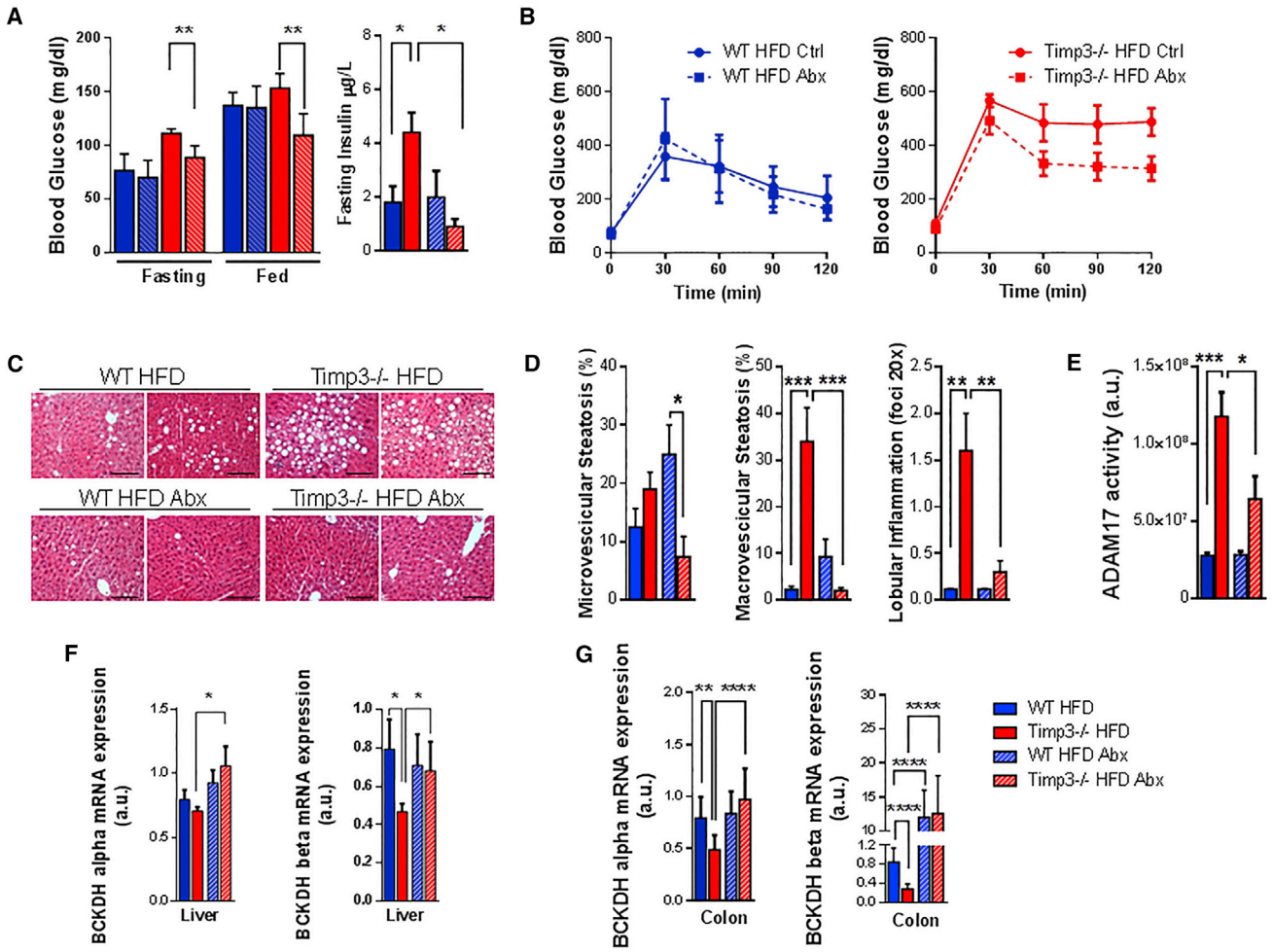

Figure 5. Antibiotic Treatment Improves Features of Metabolic Syndrome, Low-Grade Inflammation, and ADAM17 Activity in Timp3$^{-/-}$ Mice Fed an HFD

(A) Fasting and fed blood glucose levels (left) (n = 6 per group; data are mean ± SEM; Student's t test with Welch's correction **p < 0.01) and fasting insulin level (right) in antibiotic-treated WT and Timp3$^{-/-}$ mice fed an HFD compared to untreated controls (n = 6 per group; data are mean ± SEM; one-way ANOVA with Tukey's multiple comparison test; *p < 0.05 per fasting insulin.

(B) IPGTT test of WT (left) and Timp3$^{-/-}$ mice (right) after in vivo antibiotic treatment compared to an untreated control.

(C and D) Histology of liver in WT (left) and Timp3$^{-/-}$ mice fed an HFD (right) (H&E stain; scale bar, µm) after antibiotic treatment compared with untreated controls (C) and the percentage of microvescicular, macrovescicular, and lobular inflammation (D) (n = 4–5 per group; data are mean ± SEM; one-way ANOVA with Sidak's multiple comparison test; *p < 0.05, **p < 0.01, ***p < 0.001).

(E) ADAM17 activity in untreated WT and Timp3$^{-/-}$ mice fed an HFD compared with antibiotic-treated littermates (n = 5 per group; data are mean ± SEM; one-way ANOVA with Sidak's multiple comparisons test; *p < 0.05, ***p < 0.001).

(F and G) mRNA expression of BCKDHα and BCKDHβ subunits in liver (F) and colon (G) before and after antibiotic treatment (Abx) in WT and Timp3$^{-/-}$ mice fed an HFD (n = 9 for colon analysis; n = 5 for liver analysis; data are mean ± SEM; *p < 0.05 **p < 0.01, ****p < 0.0001 by Mann-Whitney t test).

See also Figure S6 and Tables S4, S5, S6, S7, and S8.

steatosis, inflammation, ADAM17 convertase, and MMPs activities in Timp3$^{-/-}$ mice (Figures 7G–7I and S7B).

DISCUSSION

We have identified a pathway coordinated by Timp3 active at the gut level. Gut dysbiosis in Timp3-null mice leads to liver steatosis and the release of soluble IL6R. In turn, increased sIL6R results in the accumulation of CD11c^{+} cells in peripheral tissues and in insulin resistance.

Data from other models clearly showed that activation of inflammatory pathways at the gut level has a broad role in glucose homeostasis at the systemic level (Cox et al., 2015; Denou et al., 2015; Duca et al., 2014; Everard et al., 2013; Tremaroli and Bäckhed, 2012). The mechanistic role of the intestinal immune system as a primary sensor in the cross-talk between nutrients, gut microbes, and hosts in metabolic disorders has been recently identified (Everard et al., 2014).

In previous analysis we showed that the interaction of Timp3 deficiency with genetic insulin resistance during a short dietary

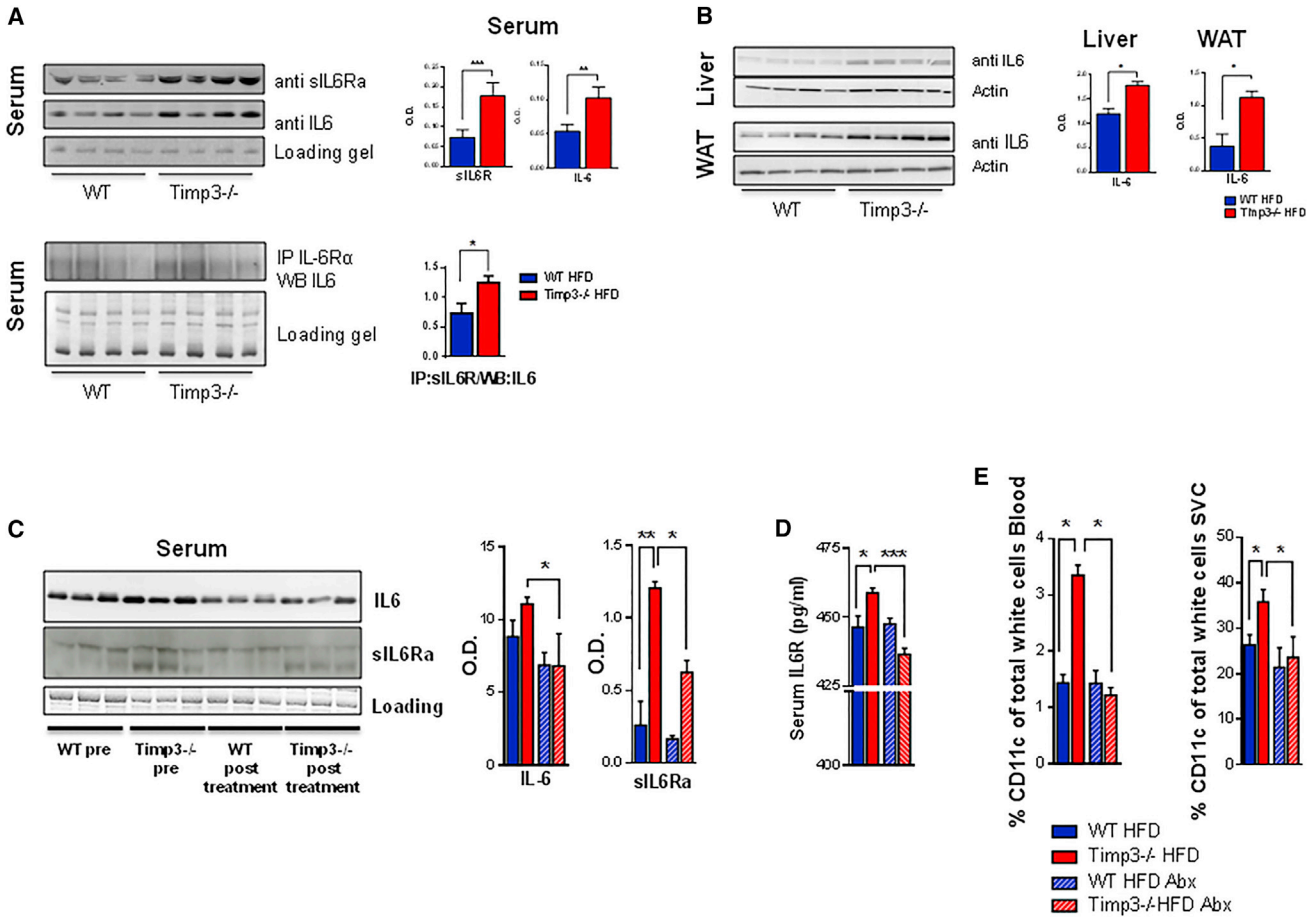

Figure 6. IL-6 and sIL6R Levels in Blood, Liver, and WAT

(A) Serum levels of IL-6 and sIL6Rα analyzed by western blot (left) and graphic representation of optical density (OD) of IL-6 and sIL6R protein levels in serum, which were normalized to loading (right) (n = 4 per group; data are mean ± SEM; one-way ANOVA with Sidak's multiple comparison test; *p < 0.05, **p < 0.01, ***p < 0.001).

(B) IL-6 expression analyzed by western blot in liver and WAT of WT and Timp3$^{-/-}$ mice fed an HFD (left) and graphic representation of optical density (OD) (n = 4 data are mean ± SEM; *p < 0.05 by Mann-Whitney t test.

(C) Serum levels of IL-6 and sIL6Rα protein levels in untreated WT and Timp3$^{-/-}$ mice fed an HFD compared with antibiotic-treated littermates analyzed by western blot (left) and graphic representation of optical density (OD), which were normalized to loading (right) (n = 3 per group; data are mean ± SEM; one-way ANOVA with Sidak's multiple comparison test *p < 0.05; **p < 0.01).

(D) ELISA of sIL6R in sera of untreated WT and Timp3$^{-/-}$ mice fed an HFD compared with antibiotic-treated littermates. (n = 4 per group; data are mean ± SEM; one-way ANOVA with Sidak's multiple comparison test; *p < 0.05, ***p < 0.001).

(E) Flow cytometry analysis of blood leukocyte and stromal vascular cells (SVCs) was performed using monoclonal antibodies directed against dendritic cells (CD11c^{+}). In antibiotic-treated Timp3$^{-/-}$ mice fed an HFD we found a decrease in the percentage of CD11c^{+} population compared with littermate controls, whereas no difference was found in treated WT mice fed an HFD compared with the control after 4 weeks of antibiotic treatment (Abx) (n = 5 per group; data are mean ± SEM. *p < 0.05 by Mann-Whitney t test, a.u.).

challenge, as well as loss of Timp3 in a prolonged dietary challenge resulted in associated increased expression of both inflammatory and de novo lipogenic genes, such as IL-6 and SCD-1 (Fiorentino et al., 2010; Menghini et al., 2009). However, these studies neither clarified how the nutritional stimulus was reflected into metabolic inflammation in vivo nor determined whether a tissue is affected first and consequently spreads signals to others.

It has been recently shown that sIL6R is involved in CD11c^{+} accumulation in WAT despite an apparently minor effect on insulin resistance. However, which signals are upstream of the hyperactivation of the sIL6R trans-signaling pathway from the liver to periphery remained untested (Kraakman et al., 2015). Our data help to fill these gaps.

We show that sIL6R is higher in concomitance of the loss of Timp3. Our work suggests that gut dysbiosis, independent of gut bacterial translocation, affects both liver steatosis and the release of sIL6R to activate IL-6 trans-signaling and CD11c^{+} recruitment pathway. Whether this axis is acting specifically at the liver level or whether other tissues contribute remains to be established in future works with targeted models.

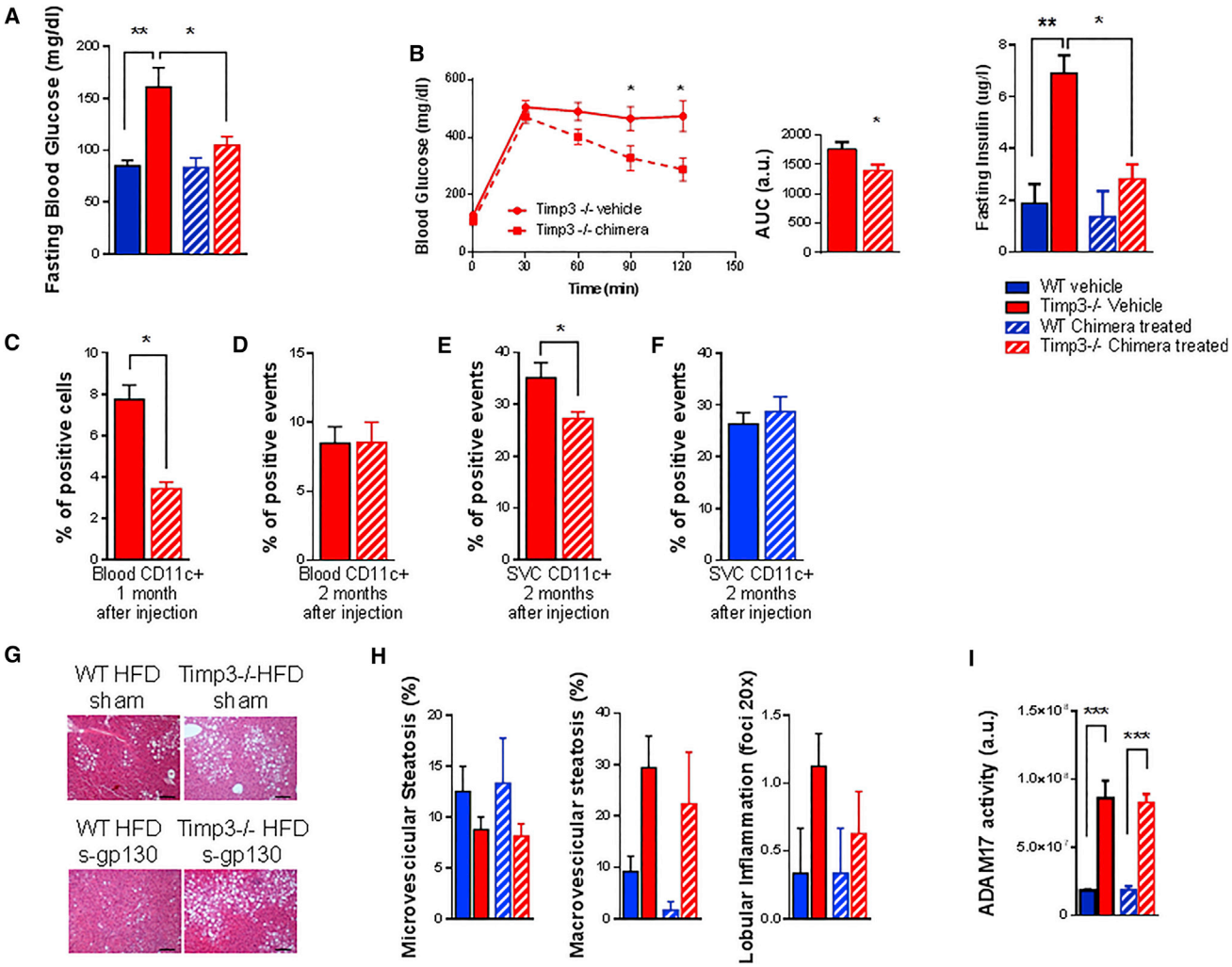

Figure 7. Inhibition of sIL6R Signaling Controls CD11c$^+$ Trafficking with Mild Effects on Glucose Tolerance and No Effect on Steatosis and ADAM17 Activity

(A) Soluble gp130Fc (sgp130Fc) effect on metabolic status: fasting blood glucose 1 month post-injection in WT and Timp3$^{-/-}$ mice fed an HFD injected with sgp130Fc (chimera) compared with littermates injected with PBS (vehicle) (n = 4 data are mean ± SEM; one-way ANOVA with Sidak's multiple comparison test; *p < 0.05, **p < 0.01.

(B) Intraperitoneal glucose tolerance test and area under curve (AUC) (left) and fasting insulin level (right) after two months from in vivo treatment of Timp3$^{-/-}$ mice with sgp130Fc (chimera) compared with Timp3$^{-/-}$ mice fed an HFD and injected with PBS (vehicle). (n = 9; data are mean ± SEM; *p < 0.05 by Mann-Whitney t test; a.u. per AUC; one-way ANOVA with Sidak's multiple comparison test per fasting insulin; *p < 0.05, **p < 0.01).

(C–F) Effect on CD11c$^+$ cells in blood at 1 month (C) and 2 months (D) and in SVC at 2 months (E) after injection of soluble gp130Fc in Timp3$^{-/-}$ mice and in SVC at 2 months (F) after injection of soluble gp130Fc in WT mice (n = 4/each group; Bonferroni's test *p < 0.05).

(G and H) Histology of liver in WT and Timp3$^{-/-}$ mice fed an HFD (H&E stain: scale bar, μm) after treatment compared with littermate controls (G) and the percentage of microvescicular, macrovescicular, and lobular inflammation (H).

(I) ADAM17 activity in WT and Timp3$^{-/-}$ mice fed an HFD and injected with sgp130Fc (chimera) compared with littermates injected with PBS (vehicle) (n = 4 data are mean ± SEM; one-way ANOVA with Sidak's multiple comparison test; ***p < 0.001).

See also Figure S7.

The role of CD11c$^+$ accumulation as part of the ATM burden in obesity and the consequent effect on glucose intolerance has been recently discussed (Patsouris et al., 2008; Wentworth et al., 2010; Wu et al., 2010). Our results are in accordance with those of Kraakman et al. (2015) by showing that the insulin-sensitizing effect of sgp130Fc is mild and less efficacious compared with antibiotic treatment, despite a strong preventive effect on SVC-CD11c$^+$ accumulation in both cases. However, we cannot exclude that the CD11c$^+$ cells have insulin resistance effects in tissues other than WAT or that sub-types of CD11c$^+$ cells exhibit different phenotypes (Li et al., 2010; Wentworth et al., 2010). Our data support that CD11c$^+$ accumulation in ATM is part of a broader scenario in which changes in gut-related metabolites may influence glucose metabolism and that immune

cells accumulate at the peripheral level as part of a systemic response.

Our data also point to the regulation of the interaction between the gut immune system and nutrients as a more efficacious target for the control of glucose homeostasis rather than the adipose immune system. Which agents trigger local inflammation remains unknown, although it is tempting to speculate about the possible influence of gut microbiome-related metabolites.

Several groups have investigated the link between gut microbiome, the associated metabolites, and the influence on host metabolism. Short chain fatty acids (SCFA) have been long considered a major driver to preserve insulin sensitivity as a response to changes in bacterial genus, such as *Roseburia* and *Faecalibacterium prausnitzii*. SCFA released from the gut may interact with GPR41 to affect adipose tissue metabolism (Karlsson et al., 2013).

Our metabolomics screening unveils a potential role for aromatic amino acid derivatives, generally considered important as uremic toxins, also in early phases of insulin resistance (Koppe et al., 2013; Lustgarten et al., 2014). However, the increase in indole compounds, particulary indoxylsulfate, is consistent with accumulation of uremic toxins as an effect of diabetic nephropathy observed in Timp3$^{-/-}$ (Fiorentino et al., 2013a; Fiorentino et al., 2013b).

Branched chain amino acids (BCAAs) have been also associated with insulin resistance and cardiovascular disorders in human subjects (Laferrère et al., 2011; Lynch and Adams, 2014; Newgard et al., 2009). The basis for defective BCAA metabolism in metabolic disorders, such as obesity, diabetes, and atherosclerosis, is still a matter of debate. Our data show that BCKDH, the rate-limiting enzyme in BCAA metabolism, is downregulated in a model combining nutrient excess to Timp3 deficiency. However, antibiotic treatment reverses this defect, suggesting a link between gut dysbiosis and BCAA metabolism, particularly in the colon itself and in the liver.

The gut microbiota is now accepted as a major component in metabolic disorders independent of genetics, as well as a plausible cause to explain how social changes in only one century has so dramatically increased the prevalence of obesity and related complications (Ridaura et al., 2013). Knowledge of gut microbiome is still poor, although recent studies have identified some bacterial genus and species causally linked to the onset of obesity and diabetes.

We have previously shown that Timp3$^{-/-}$ mice suffer from increased susceptibility to inflammatory bowel disease, where the gut microbiome may also play a part (Monteleone et al., 2012). The role of innate immune mechanisms in regulating metabolic disorders through modulation of gut microbiota was reported in models with deletion of crucial pattern recognition receptors (TLR2, TLR4, and TLR5) or adaptors, such as (Myd88) (Kellermayer et al., 2011; Kim et al., 2012; Vijay-Kumar et al., 2010). Ablation of TLR2 in mice fed an HFD under germ-free conditions increases the risk of metabolic syndrome, particularly through regulation of Firmicutes and increased LPS absorption. In our results we found that TIMP3 modulates the gut microbiota at family levels, suggesting a different way to affect host-microbial interactions. Because antibiotics, but not sgp130fc chimera treatment, dampened ADAM17 activity in the liver (although we cannot exclude that other tissues are also affected in a similar manner), it is intriguing to speculate about a role for gut microbiome-related metabolites on ADAM17. However, our results do not allow us to discriminate whether the increased activity of ADAM17 is a direct effect of gut microbiome metabolism or whether other messengers mediate this effect.

A limitation of the present results is that our data do not clarify whether TIMP3 has a direct role on the metabolic abnormalities or whether TIMP3-related gut dysbiosis mediate metabolic abnormalities independent from TIMP3. To discern between these possibilities, future studies must be performed to address whether dysbiotic microbiota transplantation from Timp3$^{-/-}$ to WT mice is sufficient to induce phenotype in WT mice, eventually using co-housing approach.

Our data suggest that beside the paradigm of bacterial translocation as an essential step for development of obesity and its consequences, an alternative model characterized by metabolically active dysbiosis exists and should be exploited in human subjects with diabetes.

In conclusion, we observed that TIMP3 affects gut microbiome-related liver steatosis and glucose intolerance in mice challenged with nutrient excess, suggesting that modulation of the gut microbiome via TIMP3 is a new possible mechanism to improve glucose intolerance status.

EXPERIMENTAL PROCEDURES

Mouse Model and Metabolic Tests

Timp3$^{-/-}$ mice on a C57/BL6 background, as well as the metabolic testing procedures, have been previously described (Federici et al., 2005; Menghini et al., 2009; Mohammed et al., 2004; Serino et al., 2007). All animal procedures are in accordance with the Guide for the Care and Use of Laboratory Animals published by the NIH (publication no. 85–23, revised 1996), approved by the University Hospital of Tor Vergata Animal Care Facility, and have been previously described (Fiorentino et al., 2013a).

WT and Timp3$^{-/-}$ mice lines were housed in separated cages, with each cage containing 3–4 mice of the same genotype and fed an HFD (HFD) (60% of calories from fat; Research Diets) or normal diet (ND) (10% calories from fat, Good Laboratory Practices [GLP]; Mucedola S.r.l.) for 16 weeks after weaning. The sgp130Fc was administered in the same conditions as above, starting at week 8 of the HFD and ending at week 16 of the HFD.

After 12 weeks on an HFD, mice (in the same conditions as above) were separated in isolated autoclaved cages (one mouse per cage), and antibiotics were administered in the water for a duration of 4 weeks, while the HFD regimen was maintained. All the disposals used during the antibiotic treatment were sterile.

Serum Measurements

ELISA was performed for the soluble IL-6 receptor (MyBioSource); plasma insulin was assessed using an ultrasensitive mouse insulin ELISA kit (Mrcodia) in accordance with the manufacturer's instructions. The remaining samples were stored in appropriate (endotoxin-free) vials at −80°C until the endotoxin analysis, which was performed using a commercially available kit (limulus amebocyte lysate [LAL], Chromogenic Endpoint Assay, Hycult Biotechnology). To neutralize endotoxin inhibitors, serum was heated at 70°C for 30 min before being processed.

ADAM17 Activity

ADAM17 activity was determined using the SensoLyte 520 TACE Activity Assay Kit (AnaSpec), in accordance with the manufacturer's protocol. 30 μg of tissue proteins were used for the assay. Reaction was started by adding 40 μM of the fluorophoric QXL520/5FAM FRET substrate. Fluorescence of

the cleavage product was measured in a fluorescence microplate reader (Beckman Coulter DTX 800) at lex 490 nm and lem 520 nm.

Assay Citokine

The cytokines and chemokines profiles of the sera mouse were analyzed using RayBio Mouse Cytokine Antibody Array (Cat# AAM-CYT-3, RayBiotech), in accordance with the manufacturer's instruction.

Isolation of Adipocytes and SVF

White adipose tissue (WAT) separation was performed as previously described (Fabrizi et al., 2014).

Flow Cytometry Analysis

Cells from the stromal vascular fraction (SVF) of adipose tissue and blood cells were stained with CD11c (Milteny Biotec), CD11b (Miltenyi Biotec), F4/80 (Miltenyi Biotec), and CX3CR1 (R&D System). For the blood, in brief, 200 μl were collected retro-orbitally and anticoagulated with heparin. Red blood cells were lysed with RBC Lysis Buffer (EBioscience) and then stained with fluorescently labeled primary antibodies.

Samples were analyzed using a FACScalibur (BD Bioscience) running BD Cellquest Pro and analyzed with Flow JO (TreeStar). Monocytes were defined as $CX3CR1^{+}$ and $CD11b^{+}$, whereas subpopulations of macrophages were defined as $F4/80^{+}CX3CR1^{-}$, and dendritic cells were defined as CD11c total and $CD11c^{+}CX3CR1^{+}$ and $CX3CR1^{-}$.

Gene Expression Analysis by qRT-PCR

Total RNA was isolated from tissue using TRIzol Reagent (Invitrogen). 2 μg of total RNA were reverse transcribed into cDNA using the High Capacity cDNA Archive Kit (Applied Biosystems). A quantitative real-time PCR was performed using an ABI PRISM 7700 System and TaqMan reagents (Applied Biosystems). Each reaction was performed in triplicate using standard reaction conditions, and the cycle threshold (Ct) value was normalized in mouse by β-actin.

Western Blot

Preparation of tissue lysates, quantification, and immunoblot analysis were performed as previously described (Marino et al., 2014). Antibodies to IL-6 (Invitrogen), sIL6R (R&D Systems), and actin (Santa Cruz Biotechnology) were used.

Metabolomics Analysis

Targeted global metabolomic analysis was carried out by Metabolon. See the Supplemental Experimental Procedures for a complete description of methods.

Histological Analysis

Liver and intestinal tissues were obtained from mice fed an HFD; specimens were fixed in10% paraformaldehyde and embedded in paraffin. 10-μm consecutive sections were then mounted on slides and stained with H&E (Sigma-Aldrich).

The severity of nonalcoholic fatty liver disease was based on the amount and types of fat (macrovescicular and microvescicular), extent of inflammation, presence of cell degeneration (acidophil bodies, ballooning, and Mallory's hyaline), or necrosis and degree of fibrosis as described.

16S rRNA and Metagenomics Analysis

The caecal content was collected postmortem from each mouse (five/group) and was stored at −80°C.

The DNA was extracted from the caecal content of mice using the QIAamp DNA Stool Mini Kit (QIAGEN), in accordance with the manufacturer's instructions.

Microbial community composition was assessed by sequencing hypervariable regions (HVR) 5–6 of the 16S rRNA (GENOMNIA, EBI metagenomics: PRJEB8244) derived from caecal samples of both chow diet (ND) and high-fat diet (HFD) animals.

Antibiotics Treatment

After 4 months on an HFD, WT and $Timp3^{-/-}$ mice were subjected to antibiotics treatment. Norfloxacin, metronidazole, and ampicillin (1 g/l each) (Sigma Aldrich) were added to the drinking water for 4 weeks as previously described (Denou et al., 2015).

Injection of the Soluble Form of gp130Fc-Protein

WT and $Timp3^{-/-}$ mice (n = 20/each) fed an HFD for 2 months were injected intraperitoneally twice with a solution (20 μg/animal) of the soluble form of gp130Fc (R&D Systems).

Glycaemia were routinely checked in fasted and fed animals. After injection, the number of circulating myeloid cells (as CD11c, CD11b, CX3CR1, and F4/80) was determined by flow cytometry.

Statistical Analysis

Results of the experimental studies are expressed as means ± SEM. Statistical analyses were performed with GraphPad Prism (v.6.02) and R (v.3.0.2). Groups were compared using a two-tailed unpaired Student's t test and Mann-Whitney test; one- or two-way ANOVA with post hoc comparisons is as indicated. Multiplicity was taken into account by means of Benjamini and Hochberg correction, and hence the threshold for significance is data dependent. In this context, Benjamini and Hochberg (1995) correction guarantees a false discovery rate below 0.05 (Farcomeni, 2006, 2007, 2008). Linear correlation analysis was performed using the Spearman test. Values of $p < 0.05$ have been considered statistically significant. Pathway analysis was performed by means of functional class scoring (FCS): gene-level statistics (p values from one or two-way ANOVA) have been aggregated by means of the median, and then the statistical significance of the pathway has been assessed by means of permutation. The top-ten pathways are considered as worth mentioning and further investigating (Qureshi and Sacan, 2013; Khatri et al., 2012).

ACCESSION NUMBERS

The accession number for the EBI metagenomics reported in this paper is PRJEB8244.

SUPPLEMENTAL INFORMATION

Supplemental Information includes Supplemental Experimental Procedures, seven figures, and eight tables and can be found with this article online at http://dx.doi.org/10.1016/j.celrep.2016.06.027.

AUTHOR CONTRIBUTION

M.F. conceived and supervised the study. M.M. and V.M designed the experiments, interpreted the results, and generated the figures and tables. M.F., R.M., and M.M. wrote the manuscript. R.S., L.F., A.M., V.C., G.M., I.M., M.F., A.M., and M.C. performed the experiments. R.B. and C.G. performed and analyzed the results from bacterial traslocation. A.F. and B.K. performed the statistical analysis on metabolomics data and contributed to data interpretation. All authors discussed the data and commented on the manuscript before submission.

ACKNOWLEDGMENTS

This manuscript was funded in part by FP7-FLORINASH grant agreement HEALTH-F2-2009-241913, the EFSD Lilly Project 2013, the Associazione Italiana per la Ricerca sul Cancro (AIRC IG-13163), the MIUR PRIN (20123BJ89E), and the Fondazione Roma Non Communicable Diseases 2014 Call (to M.F.).

Received: November 3, 2015
Revised: March 23, 2016
Accepted: June 3, 2016
Published: June 30, 2016

REFERENCES

Anstee, Q.M., Targher, G., and Day, C.P. (2013). Progression of NAFLD to diabetes mellitus, cardiovascular disease or cirrhosis. Nat. Rev. Gastroenterol. Hepatol. *10*, 330–344.

Benjamini, Y., and Hochberg, Y. (1995). Controlling the false discovery rate: a practical and powerful approach to multiple testing. J. R. Stat. Soc. B *57*, 289–300.

Cardellini, M., Menghini, R., Martelli, E., Casagrande, V., Marino, A., Rizza, S., Porzio, O., Mauriello, A., Solini, A., Ippoliti, A., et al. (2009). TIMP3 is reduced in atherosclerotic plaques from subjects with type 2 diabetes and increased by SirT1. Diabetes *58*, 2396–2401.

Cardellini, M., Menghini, R., Luzi, A., Davato, F., Cardolini, I., D'Alfonso, R., Gentileschi, P., Rizza, S., Marini, M.A., Porzio, O., et al. (2011). Decreased IRS2 and TIMP3 expression in monocytes from offspring of type 2 diabetic patients is correlated with insulin resistance and increased intima-media thickness. Diabetes *60*, 3265–3270.

Casagrande, V., Menghini, R., Menini, S., Marino, A., Marchetti, V., Cavalera, M., Fabrizi, M., Hribal, M.L., Pugliese, G., Gentileschi, P., et al. (2012). Overexpression of tissue inhibitor of metalloproteinase 3 in macrophages reduces atherosclerosis in low-density lipoprotein receptor knockout mice. Arterioscler. Thromb. Vasc. Biol. *32*, 74–81.

Cox, A.J., West, N.P., and Cripps, A.W. (2015). Obesity, inflammation, and the gut microbiota. Lancet Diabetes Endocrinol. *3*, 207–215.

Denou, E., Lolmède, K., Garidou, L., Pomie, C., Chabo, C., Lau, T.C., Fullerton, M.D., Nigro, G., Zakaroff-Girard, A., Luche, E., et al. (2015). Defective NOD2 peptidoglycan sensing promotes diet-induced inflammation, dysbiosis, and insulin resistance. EMBO Mol. Med. *7*, 259–274.

Duca, F.A., Sakar, Y., Lepage, P., Devime, F., Langelier, B., Doré, J., and Covasa, M. (2014). Replication of obesity and associated signaling pathways through transfer of microbiota from obese-prone rats. Diabetes *63*, 1624–1636.

Everard, A., Belzer, C., Geurts, L., Ouwerkerk, J.P., Druart, C., Bindels, L.B., Guiot, Y., Derrien, M., Muccioli, G.G., Delzenne, N.M., et al. (2013). Cross-talk between Akkermansia muciniphila and intestinal epithelium controls diet-induced obesity. Proc. Natl. Acad. Sci. USA *110*, 9066–9071.

Everard, A., Geurts, L., Caesar, R., Van Hul, M., Matamoros, S., Duparc, T., Denis, R.G., Cochez, P., Pierard, F., Castel, J., et al. (2014). Intestinal epithelial MyD88 is a sensor switching host metabolism towards obesity according to nutritional status. Nat. Commun. *5*, 5648.

Fabrizi, M., Marchetti, V., Mavilio, M., Marino, A., Casagrande, V., Cavalera, M., Moreno-Navarrete, J.M., Mezza, T., Sorice, G.P., Fiorentino, L., et al. (2014). IL-21 is a major negative regulator of IRF4-dependent lipolysis affecting Tregs in adipose tissue and systemic insulin sensitivity. Diabetes *63*, 2086–2096.

Farcomeni, A. (2006). More powerful control of the false discovery rate under dependence. Stat. Methods Appl. *15*, 43–73.

Farcomeni, A. (2007). Some results on the control of the false discovery rate under dependence. Scand. J. Stat. *34*, 275–297.

Farcomeni, A. (2008). A review of modern multiple hypothesis testing, with particular attention to the false discovery proportion. Stat. Methods Med. Res. *17*, 347–388.

Federici, M., Hribal, M.L., Menghini, R., Kanno, H., Marchetti, V., Porzio, O., Sunnarborg, S.W., Rizza, S., Serino, M., Cunsolo, V., et al. (2005). Timp3 deficiency in insulin receptor-haploinsufficient mice promotes diabetes and vascular inflammation via increased TNF-alpha. J. Clin. Invest. *115*, 3494–3505.

Ferrante, A.W., Jr. (2013). Macrophages, fat, and the emergence of immunometabolism. J. Clin. Invest. *123*, 4992–4993.

Fiorentino, L., Vivanti, A., Cavalera, M., Marzano, V., Ronci, M., Fabrizi, M., Menini, S., Pugliese, G., Menghini, R., Khokha, R., et al. (2010). Increased tumor necrosis factor alpha-converting enzyme activity induces insulin resistance and hepatosteatosis in mice. Hepatology *51*, 103–110.

Fiorentino, L., Cavalera, M., Mavilio, M., Conserva, F., Menghini, R., Gesualdo, L., and Federici, M. (2013a). Regulation of TIMP3 in diabetic nephropathy: a role for microRNAs. Acta Diabetol. *50*, 965–969.

Fiorentino, L., Cavalera, M., Menini, S., Marchetti, V., Mavilio, M., Fabrizi, M., Conserva, F., Casagrande, V., Menghini, R., Pontrelli, P., et al. (2013b). Loss of TIMP3 underlies diabetic nephropathy via FoxO1/STAT1 interplay. EMBO Mol. Med. *5*, 441–455.

Johnson, A.M., and Olefsky, J.M. (2013). The origins and drivers of insulin resistance. Cell *152*, 673–684.

Karlsson, F.H., Tremaroli, V., Nookaew, I., Bergström, G., Behre, C.J., Fagerberg, B., Nielsen, J., and Bäckhed, F. (2013). Gut metagenome in European women with normal, impaired and diabetic glucose control. Nature *498*, 99–103.

Kellermayer, R., Dowd, S.E., Harris, R.A., Balasa, A., Schaible, T.D., Wolcott, R.D., Tatevian, N., Szigeti, R., Li, Z., Versalovic, J., and Smith, C.W. (2011). Colonic mucosal DNA methylation, immune response, and microbiome patterns in Toll-like receptor 2-knockout mice. FASEB J. *25*, 1449–1460.

Khan, M.T., Nieuwdorp, M., and Bäckhed, F. (2014). Microbial modulation of insulin sensitivity. Cell Metab. *20*, 753–760.

Khatri, P., Sirota, M., and Butte, A.J. (2012). Ten years of pathway analysis: current approaches and outstanding challenges. PLoS Comput. Biol. *8*, e1002375.

Kim, K.A., Gu, W., Lee, I.A., Joh, E.H., and Kim, D.H. (2012). High fat diet-induced gut microbiota exacerbates inflammation and obesity in mice via the TLR4 signaling pathway. PLoS ONE *7*, e47713.

Koppe, L., Pillon, N.J., Vella, R.E., Croze, M.L., Pelletier, C.C., Chambert, S., Massy, Z., Glorieux, G., Vanholder, R., Dugenet, Y., et al. (2013). p-Cresyl sulfate promotes insulin resistance associated with CKD. J. Am. Soc. Nephrol. *24*, 88–99.

Kraakman, M.J., Kammoun, H.L., Allen, T.L., Deswaerte, V., Henstridge, D.C., Estevez, E., Matthews, V.B., Neill, B., White, D.A., Murphy, A.J., et al. (2015). Blocking IL-6 trans-signaling prevents high-fat diet-induced adipose tissue macrophage recruitment but does not improve insulin resistance. Cell Metab. *21*, 403–416.

Laferrère, B., Reilly, D., Arias, S., Swerdlow, N., Gorroochurn, P., Bawa, B., Bose, M., Teixeira, J., Stevens, R.D., Wenner, B.R., et al. (2011). Differential metabolic impact of gastric bypass surgery versus dietary intervention in obese diabetic subjects despite identical weight loss. Sci. Transl. Med. *3*, 80re2.

Li, P., Lu, M., Nguyen, M.T., Bae, E.J., Chapman, J., Feng, D., Hawkins, M., Pessin, J.E., Sears, D.D., Nguyen, A.K., et al. (2010). Functional heterogeneity of CD11c-positive adipose tissue macrophages in diet-induced obese mice. J. Biol. Chem. *285*, 15333–15345.

Lustgarten, M.S., Price, L.L., Chalé, A., and Fielding, R.A. (2014). Metabolites related to gut bacterial metabolism, peroxisome proliferator-activated receptor-alpha activation, and insulin sensitivity are associated with physical function in functionally-limited older adults. Aging Cell *13*, 918–925.

Lynch, C.J., and Adams, S.H. (2014). Branched-chain amino acids in metabolic signalling and insulin resistance. Nat. Rev. Endocrinol. *10*, 723–736.

Marino, A., Menghini, R., Fabrizi, M., Casagrande, V., Mavilio, M., Stoehr, R., Candi, E., Mauriello, A., Moreno-Navarrete, J.M., Gómez-Serrano, M., et al. (2014). ITCH deficiency protects from diet-induced obesity. Diabetes *63*, 550–561.

McNelis, J.C., and Olefsky, J.M. (2014). Macrophages, immunity, and metabolic disease. Immunity *41*, 36–48.

Mehal, W.Z. (2013). The Gordian Knot of dysbiosis, obesity and NAFLD. Nat. Rev. Gastroenterol. Hepatol. *10*, 637–644.

Menghini, R., Menini, S., Amoruso, R., Fiorentino, L., Casagrande, V., Marzano, V., Tornei, F., Bertucci, P., Iacobini, C., Serino, M., et al. (2009). Tissue inhibitor of metalloproteinase 3 deficiency causes hepatic steatosis and adipose tissue inflammation in mice. Gastroenterology *136*, 663–672.e4.

Menghini, R., Casagrande, V., Menini, S., Marino, A., Marzano, V., Hribal, M.L., Gentileschi, P., Lauro, D., Schillaci, O., Pugliese, G., et al. (2012). TIMP3 overexpression in macrophages protects from insulin resistance, adipose inflammation, and nonalcoholic fatty liver disease in mice. Diabetes *61*, 454–462.

Mohammed, F.F., Smookler, D.S., Taylor, S.E., Fingleton, B., Kassiri, Z., Sanchez, O.H., English, J.L., Matrisian, L.M., Au, B., Yeh, W.C., and Khokha, R.

(2004). Abnormal TNF activity in Timp3-/- mice leads to chronic hepatic inflammation and failure of liver regeneration. Nat. Genet. *36*, 969–977.

Monteleone, I., Federici, M., Sarra, M., Franzè, E., Casagrande, V., Zorzi, F., Cavalera, M., Rizzo, A., Lauro, R., Pallone, F., et al. (2012). Tissue inhibitor of metalloproteinase-3 regulates inflammation in human and mouse intestine. Gastroenterology *143*, 1277–1287.e1, 4.

Moschen, A.R., Kaser, S., and Tilg, H. (2013). Non-alcoholic steatohepatitis: a microbiota-driven disease. Trends Endocrinol. Metab. *24*, 537–545.

Murphy, G., Murthy, A., and Khokha, R. (2008). Clipping, shedding and RIPping keep immunity on cue. Trends Immunol. *29*, 75–82.

Newgard, C.B., An, J., Bain, J.R., Muehlbauer, M.J., Stevens, R.D., Lien, L.F., Haqq, A.M., Shah, S.H., Arlotto, M., Slentz, C.A., et al. (2009). A branched-chain amino acid-related metabolic signature that differentiates obese and lean humans and contributes to insulin resistance. Cell Metab. *9*, 311–326.

Patsouris, D., Li, P.P., Thapar, D., Chapman, J., Olefsky, J.M., and Neels, J.G. (2008). Ablation of CD11c-positive cells normalizes insulin sensitivity in obese insulin resistant animals. Cell Metab. *8*, 301–309.

Qureshi, R., and Sacan, A. (2013). Weighted set enrichment of gene expression data. BMC Syst. Biol. *7* (*Suppl 4*), S10.

Ridaura, V.K., Faith, J.J., Rey, F.E., Cheng, J., Duncan, A.E., Kau, A.L., Griffin, N.W., Lombard, V., Henrissat, B., Bain, J.R., et al. (2013). Gut microbiota from twins discordant for obesity modulate metabolism in mice. Science *341*, 1241214.

Scheller, J., Garbers, C., and Rose-John, S. (2014). Interleukin-6: from basic biology to selective blockade of pro-inflammatory activities. Semin. Immunol. *26*, 2–12.

Schumacher, N., Meyer, D., Mauermann, A., von der Heyde, J., Wolf, J., Schwarz, J., Knittler, K., Murphy, G., Michalek, M., Garbers, C., et al. (2015). Shedding of endogenous interleukin-6 receptor (IL-6R) is governed by a disintegrin and metalloproteinase (ADAM) proteases while a full-length IL-6R isoform localizes to circulating microvesicles. J. Biol. Chem. *290*, 26059–26071.

Serino, M., Menghini, R., Fiorentino, L., Amoruso, R., Mauriello, A., Lauro, D., Sbraccia, P., Hribal, M.L., Lauro, R., and Federici, M. (2007). Mice heterozygous for tumor necrosis factor-alpha converting enzyme are protected from obesity-induced insulin resistance and diabetes. Diabetes *56*, 2541–2546.

Tilg, H., and Kaser, A. (2011). Gut microbiome, obesity, and metabolic dysfunction. J. Clin. Invest. *121*, 2126–2132.

Tremaroli, V., and Bäckhed, F. (2012). Functional interactions between the gut microbiota and host metabolism. Nature *489*, 242–249.

Vijay-Kumar, M., Aitken, J.D., Carvalho, F.A., Cullender, T.C., Mwangi, S., Srinivasan, S., Sitaraman, S.V., Knight, R., Ley, R.E., and Gewirtz, A.T. (2010). Metabolic syndrome and altered gut microbiota in mice lacking Toll-like receptor 5. Science *328*, 228–231.

Wentworth, J.M., Naselli, G., Brown, W.A., Doyle, L., Phipson, B., Smyth, G.K., Wabitsch, M., O'Brien, P.E., and Harrison, L.C. (2010). Pro-inflammatory CD11c+CD206+ adipose tissue macrophages are associated with insulin resistance in human obesity. Diabetes *59*, 1648–1656.

Wu, H., Perrard, X.D., Wang, Q., Perrard, J.L., Polsani, V.R., Jones, P.H., Smith, C.W., and Ballantyne, C.M. (2010). CD11c expression in adipose tissue and blood and its role in diet-induced obesity. Arterioscler. Thromb. Vasc. Biol. *30*, 186–192.

Yan, I., Schwarz, J., Lucke, K., Schumacher, N., Schumacher, V., Schmidt, S., Rabe, B., Saftig, P., Donners, M., Rose-John, S., et al. (2016). ADAM17 controls IL-6 signaling by cleavage of the murine IL-6Ralpha from the cell surface of leukocytes during inflammatory responses. J. Leukoc. Biol. *99*, 749–760.